ARTICLE

Engineered AAV capsids mediate transduction of murine neurofibroma and sciatic nerve

Edwina Abou Haidar[1,11], Shilpa Prabhakar[1,11], Pike See Cheah[1,2], Killian S. Hanlon[1,3,4,5], Paula Espinoza[1], Adam V. Crain[1], Nikita Patel[1], Greta W. Radcliff[1], Ming Cheng[1], Iván Coto Hernández[6], Steven Minderler[6], Demitri de la Cruz[1], Carrie Ng[1], Cintia Carla da Hora[1,7], Alain Charest[8,9], Anat Stemmer-Rachamimov[10], Nate Jowett[6], Xandra O. Breakefield[1]✉ and Casey A. Maguire[1]✉

Genetic diseases such as Neurofibromatosis type 1 (NF1) and Charcot-Marie Tooth disease involve Schwann cells (SCs) associated with peripheral nerves. Gene therapy using adeno-associated virus (AAV) vector mediated gene delivery is a promising strategy to treat these diseases. However, AAV-mediated transduction of SCs in vivo after intravascular delivery is relatively inefficient, with a lack of extensive characterization of different capsids to date. Here, we performed an in vivo selection with an AAV9 capsid peptide display library in a mouse model of NF1. We chose one capsid variant, AAV-SC3, which was present in NF1 nerves for comparison to two benchmark capsids after systemic injection. AAV-SC3 significantly outperformed one of the two benchmark capsids at levels of transgene mRNA in the neurofibroma. Immunofluorescence microscopy revealed transgene expressing Sox10-positive SCs throughout the neurofibroma with AAV-SC3 injection. Next, we performed a pooled screen with four of the top capsids from our initial selection and AAV9 and identified one capsid, AAV-SC4, with enhanced biodistribution to and transduction of normal sciatic nerve in mice. This capsid displayed a peptide with a known laminin-binding motif, which may provide a conduit for future laminin-targeting strategies. Our results provide a baseline for future AAV-based gene therapies developed for NF1 or other diseases that affect SCs.

Gene Therapy (2025) 32:385–397; https://doi.org/10.1038/s41434-025-00542-9

INTRODUCTION

Adeno-associated virus (AAV) vectors are currently the lead in vivo gene therapy system owing to their relatively efficient transduction of differentiated or slowly dividing cell types in the brain, muscle, and liver [1]. Currently, there are seven FDA- and European Medicines Agency-approved AAV-based medicines to treat genetic diseases [2–6]. Several other gene therapy trials are underway using AAV vectors for gene delivery. However, AAV is less developed for peripheral nerve transduction. In recent years, the Kleopa group has tested AAV vectors for transduction of Schwann cells (SCs) in adult mice with some success [7]. They found that AAV9 and AAVrh10 transduced SCs when transgene expression was controlled with the P0 (MPZ) promoter and delivered via intrathecal or intravenous (i.v.) injection in adult mice [7, 8]. Tanguy et al. observed that AAV9 and AAVrh10 could transduce SCs in neonatal mice via i.v. injection [9] and Homs et al. showed transduction of SCs by direct nerve injection of AAV8 [10]. We also observed transduction of sciatic nerve SCs in non-human primates (NHPs) after intrathecal injection of the engineered AAV-F capsid [11].

Neurofibroma is a benign yet complex mixed-cell tumor, composed of neoplastic SCs, axonal processes, perineurial cells, fibroblasts, endothelial cells, and immune cells (mast cells and macrophages), with excessive extracellular matrix, which develop within peripheral nerve sheaths [12]. Neurofibroma initiate due to loss of *NF1* function in the SC lineage [13], followed by a cascade of interactions with other cell types in the surrounding tumor microenvironment. There is an urgent medical need to develop therapies that address the underlying genetic abnormalities in *NF1* neurofibroma. AAV-based gene therapy to treat NF1 is one potential strategy, although there has been little to no characterization of their biodistribution and transduction in preclinical models of NF1, which may differ from other models owing to the complex nature of the cellular environment of these tumors as mentioned above.

In this study, we set out to develop AAV capsids with enhanced ability to biodistribute to and transduce neurofibroma and sciatic nerve after systemic injection of mice.

[1]Molecular Neurogenetics Unit, Department of Neurology, The Massachusetts General Hospital, Charlestown MA and Program in Neuroscience, Harvard Medical School, Boston, MA, USA. [2]Department of Human Anatomy, Faculty of Medicine and Health Sciences, Universiti Putra Malaysia, Serdang, Malaysia. [3]Department of Neurobiology, Harvard Medical School, Boston, MA, USA. [4]EGA-Institute for Women's Health, University College London, London, UK. [5]Transduction Consulting, London, UK. [6]Surgical Photonics & Engineering Laboratory, Mass Eye and Ear, Harvard Medical School, Boston, MA 02114, USA. [7]Mayo Clinic College of Medicine and Science, Jacksonville, FL 32224, USA. [8]Department of Medicine, Harvard Medical School, Boston, MA 02215, USA. [9]Cancer Research Institute, Beth Israel Deaconess Medical Center, Boston, MA 02215, USA. [10]Department of Pathology, Massachusetts General Hospital, Harvard Medical School, Boston, MA, USA. [11]These authors contributed equally: Edwina Abou Haidar, Shilpa Prabhakar.
✉email: breakefield@hms.harvard.edu; cmaguire@mgh.harvard.edu

Received: 30 April 2024 Revised: 15 May 2025 Accepted: 23 May 2025
Published online: 10 June 2025

MATERIALS AND METHODS

Cells

Human 293 T cell were obtained directly from American Type Culture Collection (CRL, 3216, Manassas, VA) and a large cryo-bank was made. Cells (passage 30 and below) were cultured in high glucose Dulbecco's modified Eagle's medium containing HEPES (Invitrogen, Carlsbad, CA) supplemented with 10% fetal bovine serum (FBS) (Sigma, St. Louis, MO) and 1x Gibco Penicillin-Streptomycin-Glutamine (100 U/mL penicillin, 100 µg/mL streptomycin, 292 µg/mL L-glutamine (Invitrogen) in a humidified atmosphere supplemented with 5% CO2 at 37 °C. Cells were tested and confirmed negative for mycoplasma contamination using a MycoAlert® kit (Lonza).

Animals

All animal experiments were approved by the Massachusetts General Hospital Subcommittee on Research Animal Care following guidelines set forth by the National Institutes of Health Guide for the Care and Use of Laboratory Animals. We used adult age (8-10 week old) female C57BL/6 (strain # 000664) from The Jackson Laboratory (Bar Harbor, ME). No sample size calculation was performed for the experiments. Sample sizes were chosen based on prior experiments which yielded statistically significant differences between groups. For all animal studies, investigators assigned to perform analysis of tissues were blinded to the group identity. The principal investigator held the key to the codes and the samples were unblinded at the time of graphing the data.

The NF1 floxed animal model was a gift from Dr. Luis Parada, UT Southwestern Medical Center, Dallas, TX with exons 31–32 of *Nf1* gene flanked by loxP sites provided by Dr. Nancy Ratner [13]. The luciferase reporter mouse strain was contributed by Dr. Alain Charest, Beth Israel Deaconess Medical Center, Boston, MA. This animal model has a loxP-flanked STOP cassette upstream of the luciferase cDNA [14]. $Nf1^{flox/flox}$/$Fluc^{flox}$ animal model was generated by mating the $Nf1^{flox/flox}$ xand $Fluc^{flox/-}$ mice with each other and genotyping of progeny.

$Nf1^{flox/flox}$/$Fluc^{flox}$ littermates were identified by tail genotyping using two sets of PCRs, targeting *Nf1* and *luciferase* genes, respectively. First PCR was used to amplify the *Nf1* gene at two sites : a 480-bp band [from intron 30 of the Nf1 gene of the wild-type (WT) allele] and a 350-bp band (from the neo gene of the floxed allele; for details refer to Supplementary Table S1). Conditions for genotyping were 94 °C for 1 min followed by 30 cycles of 94 °C for 30 s, 65 °C for 30 s and 72 °C for 60 s and ending with an extension for 2 min at 72 °C using primers targeting Nf1 (Supplementary Table S1). Another PCR was performed to detect the presence of the floxed luciferase transgene. Conditions for genotyping were 95 °C for 5 min followed by 40 cycles of 94 °C for 30 s, 55 °C for 30 s and 72 °C for 30 s and ending with an extension for 10 min at 72 °C using primers in Supplementary Table S1.

For animal studies using C57BL/6 mice, mice were randomly grouped. For the $Nf1^{flox/flox}$/$Fluc^{flox}$ mice used in the studies with vectors targeting NF1 neurofibroma, mice were grouped according to the bioluminescent signal from the AAV1-Cre injected nerve(s) as described in the section "Transduction and biodistribution study in the murine NF1 model".

AAV peptide display library production. We have previously described construction and production of the iTransduce AAV9 peptide display library [11].

AAV-P0-tdTomato (tdT) expression cassette and AAV-CAP.NF rep/cap plasmid construction. To generate an AAV expression cassette driving tdT under the P0 promoter we used pAAV-CAG-tdT (codon diversified), a gift from Edward Boyden (Addgene plasmid # 59462; http://n2t.net/addgene:59462; RRID:Addgene_59462). We removed the CAG promoter/elements using an upstream NdeI site and downstream KpnI site (upstream of tdT cDNA). Next, we PCR-amplified a fragment of rat P0 promoter (Q5 enzyme, NEB, Ipswich, MA) from dsAAV-PO-GFP plasmid [15] using the following primers which both contain sequences homologous to pAAV-CAG-tdT for Gibson Assembly:

Gibson Rat P0 For: 5′-tgcccacttggcagtacatcaagtgtatcatatgacgagcattctc-gaactct-3′

Gibson Rat P0 Rev: 5′-cctcgcccttactcaccatggtggcggtacccagagcgtctgtggggt-3′

We next performed a Gibson Assembly reaction (NEB) with the digested AAV-tdT plasmid and P0 promoter PCR product with homology arms and transformed an aliquot of the assembly into SURE electrocompetent bacteria (Agilent, Santa Clara, CA). Bacterial clones were screened by SmaI restriction enzyme digestion to evaluate inverted terminal repeat (ITR) integrity. Next, we performed complete plasmid sequencing to confirm sequence integrity using Oxford Nanopore technology at Plasmidsaurus (Eugene, OR).

To create a *rep/cap* plasmid encoding AAV9 capsids displaying the peptide inserts of interest for production of vectors encoding AAV-P0-tdTomato, we digested an AAV9 *rep/cap* plasmid with BsiWI and BaeI which removed a fragment flanking the VP3 amino acid 588 site for peptide sequence insertion. Next, we ordered a 997 bp dsDNA fragment from Integrated DNA Technologies (IDT, Coralville, IA), which contains overlapping Gibson homology arms with the BsiWI/BaeI cut AAV9 as well as the 21-mer nucleotide sequence encoding the peptide of interest in frame after amino acid 588 of VP3. Last, we performed Gibson assembly using the Gibson Assembly® Master Mix (NEB) to ligate the peptide containing insert into the AAV9 *rep/cap* plasmid. Insert identification was confirmed by complete plasmid sequencing as above.

AAV vector production, purification, and titration. For transgene expression studies we used pAAV-P0-tdT plasmid described above. AAV production was performed, as previously described [16]. Briefly, 293 T cells were triple transfected using polyethylenimine reagent with (1) rep/cap plasmid (AAV9, AAV-F, AAV-SC3, or AAV-SC4) (2) an adenovirus helper plasmid, pAdΔF6, and (3) ITR-flanked AAV-P0-tdT transgene expression plasmid. Cell lysates were harvested 68–72 h post-transfection and purified by ultracentrifugation in an iodixanol density gradient. Iodixanol was removed and buffer exchanged to phosphate buffered saline (PBS) containing 0.001% Pluronic F68 (Gibco, Thermo Fisher Scientific, Waltham, MA) using 7 kDa molecular weight cutoff Zeba™ desalting columns (Thermo Fisher Scientific). Vector was concentrated using Amicon® Ultra-2 100 kDa MWCO ultrafiltration devices (Millipore Sigma, St. Louis, MO). Vector titers in vector genome (vg)/ml were determined by Taqman qPCR in an ABI Fast 7500 Real-time PCR system (Applied Biosystems, Foster City, CA) using custom probes and primers to the tdT sequence (Supplementary Table S1) and interpolated from a standard curve made with a restriction enzyme-linearized AAV plasmid. Vectors were pipetted into single-use aliquots and stored at −80 °C until use.

Barcoded AAV capsid candidate production for screening in C57BL/6 mouse sciatic nerve

We individually packed the AAV-CBA-hFrataxin barcoded genome described in [17] in each capsid candidate (AAV-SC1 to SC4) and the AAV9 capsid. Vectors were produced, purified and titered as described above.

Bioluminescence imaging of neurofibroma progression. To induce neurofibroma formation, sciatic nerves were directly injected with AAV1-CAG-Cre vector. To visualize tumor growth in the sciatic nerve, the animals were first anesthetized with isoflurane and then injected intraperitoneally with D-luciferin (150 µg/g body weight; GoldBio Technology, St. Louis, MO). Five minutes after the injection of D-luciferin, imaging was performed using an IVIS® Spectrum optical imaging system fitted with an XGI-8 Gas Anesthesia System (Perkin Elmer, Hopkinton, MA). Bioluminescent images were acquired using the auto-exposure function. Data analysis for signal intensities and image comparisons were performed using Living Image® software (Perkin Elmer). To calculate radiance for each animal, regions of interest (ROI) were carefully drawn around each signal which is expressed as radiance (photons/sec/cm^2/steradian).

Hematoxylin and eosin (H&E) and immunohistochemistry (IHC) staining for neurofibroma. Mice were transcardially perfused with 1X PBS. Neurofibroma and naïve sciatic nerves were harvested, fixed in 10% formalin overnight and then embedded in paraffin. H&E staining was performed on deparaffinized and rehydrated tissue 5 µm thick tissue sections with established standard protocol (DFHCC Special Core at MGH). To further characterize this tumor, we performed IHC staining for SC marker Sox10 (Cat no. 66786, Proteintech, Rosemont, IL) and proliferative marker Ki67 (Cat no 790-4286, Ventana Medical Systems, Oro Valley, AZ). For Sox10 and Ki67 staining, tissue sections were deparaffinized, rehydrated, and then subjected to antigen retrieval using established protocol (DFHCC Special Histology core in MGH). Tissues were blocked by 10% goat serum in PBS before immunostaining staining using 3, 3′-diaminobenzidine (DAB), according to manufacturer's protocol with the HRP-conjugated anti-rabbit (K4010 Kit, Dako Single Stain Envision Kits, Carpinteria, CA).

In vivo selection of SC-tropic capsids. We performed two rounds of in vivo selection to identify our candidate capsids. For round one, we injected the $Nf1^{flox/flox}$/$Fluc^{flox}$ neurofibroma-bearing mice ($n = 2$) with the unselected AAV peptide library via tail vein i.v. injection at a dose of 4×10^{10} vg/mouse. Two weeks post-injection, the sciatic nerve with neurofibroma and the contralateral side (naïve nerve) were harvested for DNA isolation. We

recovered cap gene sequences via PCR from both neurofibromas and the naïve nerves. DNA was isolated using the Arcturus PicoPure DNA Extraction Kit (Applied Biosystems; Cat no.: 11815-00). Then, AAV vector DNA corresponding to the 21-mer insert-containing region was amplified by PCR using Q5® High-Fidelity DNA Polymerase (New England Biolabs, cat no: M0491, Ipswich, MA) and Library NGS primers (Supplementary Table S1).We then pooled the PCR amplified cap gene containing the inserts extracted from the neurofibroma samples and cloned them into the AAV plasmid backbone to produce vector for round two.

For the second round of selection, we injected $Nf1^{flox/flox}$/$Fluc^{flox/flox}$ neurofibroma-bearing mice ($n = 2$) with the library generated from round 1 at a dose of 1.15×10^{10} vg/mouse, via the tail vein. Two weeks post-injection, the animals were euthanized, and sciatic nerves were harvested.

Unique barcode adapters were annealed to each sample, and samples were sequenced on an Illumina MiSeq. Approximately 100,000 reads per sample were analyzed. Sequence output files were quality checked initially using FastQC (http://www.bioinformatics.babraham.ac.uk/projects/fastqc/) and analyzed using a program custom written in Python. Briefly, sequences were binned based on the presence or absence of insert; insert-containing sequences were then compared to a baseline reference sequence (AAV9-VP3), and error-free reads were tabulated based on incidences of each detected unique 21-mer insert. 21-mer inserts were translated into peptides and normalized.

Transduction and biodistribution study in the murine NF1 model. Seventeen $Nf1^{flox/flox}$/$Fluc^{flox}$ mice (both sexes were included) were injected with AAV1-CBA-Cre (CBA= chicken beta-actin promoter) vector into both sciatic nerves at the sciatic notch (34 nerves total). Mice were imaged by bioluminescence imaging as described above and 34 days later separated into four groups (one no-vector group, $n = 2$; AAV9, $n = 5$; AAV-F, $n = 5$; AAV-SC3, $n = 5$). This experiment was performed once. Animal allocation into groups: we measured the bioluminescence signal in sciatic nerves for each mouse and grouped mice such that each group had an equal number of males and females and the mean bioluminescence signal for each group was within 2-fold of the other groups. Mice were then injected with 10^{12} vg of each capsid packaging the AAV-P0-tdT genome via the tail vein. Six weeks later, mice were euthanized, and one sciatic nerve was harvested and snap frozen for RT-digital droplet (dd)PCR analysis. The other sciatic nerve was drop-fixed in buffered 3.7% formaldehyde and then cryoprotected and embedded in O.C.T. media (Tissue TEK, Sakura Finetek USA, Torrance, CA) for cryosectioning. We also snap froze brain and liver from each mouse for qPCR biodistribution of AAV genomes. All groups and samples were coded and individuals running the assays below were blinded to the sample identities.

Transduction and biodistribution studies in adult C57BL/6 mice. For comparison of AAV9 to AAV-SC4 we used $n = 6$ mice/group (both sexes were included, 3 males, 3 females). Mice were then injected via the tail vein with 10^{12} vg ($\sim 5 \times 10^{13}$ vg/kg) of each capsid packaging the AAV-P0-tdT genome. Seven weeks later, mice were euthanized, and one sciatic nerve was harvested and snap frozen for RT-ddPCR and qPCR analysis. The other sciatic nerve was drop-fixed in buffered 3.7% formaldehyde and then cryoprotected and embedded in O.C.T. media (Tissue TEK, Sakura Finetek USA, Torrance, CA) for cryosectioning. All groups and samples were coded and individuals running the assays below were blinded to the sample identities. For testing transduction of liver and sciatic nerve with AAV-SC4 capsid packaging a self-complementary (sc) CAG-GFP expression cassette, we injected $n = 3$ adult female C57BL/6 mice with a dose of 1×10^{11} vg ($\sim 5 \times 10^{12}$ vg) of vector via the tail vein. Three weeks later, mice were euthanized and liver and sciatic nerves harvested for immunofluorescence microscopy analysis of cryosections. This experiment was performed one time.

Taqman real-time qPCR for AAV genome biodistribution in brain, liver, and sciatic nerve. AAV vgs and murine genomes were co-isolated from homogenized brain, liver, and sciatic nerve tissue using a DNeasy Blood and tissue kit (Qiagen, 69504, Germantown, MD). Briefly, approximately 10 mg tissue was homogenized using 1.4 mm ceramic beads and buffer ATL (Qiagen) in a BeadBug™ homogenizer (Benchmark Scientific, Sayreville, NJ). Following homogenization, we followed the manufacturer's protocol to isolate DNA. DNA concentrations were determined using a NanoDrop spectrophotometer (Thermo Fisher Scientific). All samples were diluted to 100 ng/µl and 1 µl of sample was used for a Taqman qPCR in an ABI Fast 7500 Real-time PCR system (Applied Biosystems) using probes and primers to the tdT sequence (Supplementary Table S1) and interpolated from a standard curve made with a restriction enzyme-linearized AAV plasmid. We quantitated the amount of AAV genomes in each sample by converting the vg copies in each reaction (1 ng input DNA) to AAV genomes per µg of input DNA.

RNA extraction, cDNA synthesis and ddPCR to detect AAV transduction of neurofibroma and naïve sciatic nerves. Total RNA from sciatic nerves was extracted using the Qiagen miRNeasy Micro Kit (catalog no. 217084), and an additional DNase digestion was performed using the Qiagen RNase-free DNase set (catalog no. 79254) to ensure AAV-tdT genomic DNA digestion. Complementary DNA (cDNA) was synthesized consistently for all samples, using the SuperScript IV VILO cDNA Synthesis Master Mix (Thermo Fisher Scientific, catalog no. 11756050), according to the manufacturer's protocol.

Absolute quantification of target transcripts (copies/µl) was determined using the Automated Droplet Generator QX200 AutoDG Droplet Digital System from Bio-Rad (Hercules, CA), according to the manufacturer's instructions. The TaqMan PCR reaction mixture consists of ddPCR Supermix for Probes (No dUTP) (Bio-Rad catalog no.1863024), primers, probes and template cDNA (3 ng/µL) in a final volume of 20 µL. TaqMan probe and primers were used for tdT (codon diversified, Addgene 59462 plasmid derived seq.; forward primer, 5'- TGATGGACCTGTGATGCAGA -3'; reverse primer, 5'- GCCTGGTGGATTTCTCCTTTC -3'; probe, 5' -CGGTGGAGGCCTCC-CATCCCA-3') peptidylprolyl isomerase A (PPIA) (Mm02342430_g1), and GAPDH (Hs02786624_g1). Each assembled ddPCR reaction mixture was then loaded into the sample wells of an eight-channel disposable droplet DG32 Cartridge for QX200 (Bio-Rad, catalog no.1864108). A volume of 20 µL of droplet generation oil (Bio-Rad catalog no. 1864110) was loaded into the oil well for each channel. The plate was heat sealed with a foil seal and then placed on a conventional thermal cycler and amplified to the end point, according to the manufacturer's cycling conditions. After PCR, the 96-well PCR plate was loaded on the droplet reader (Bio-Rad) and analysis of the data was performed with QuantaSoft analysis software (Bio-Rad). Tdt expression in neurofibroma was normalized to readings for PPIA, a reference gene previously used for nerve samples [18], and expression in naïve sciatic nerve was normalized to GAPDH.

Immunofluorescence analysis of neurofibroma and naïve sciatic nerve in mice injected i.v. with AAV vectors. Sciatic nerves from mice with neurofibroma were post-fixed in 4% formaldehyde diluted in PBS for 48 h, followed by 30% (w/v) sucrose for cryopreservation for another 48–72 h after which nerves were embedded and frozen in Tissue-Tek ® O.C.T. compound (Fisher Scientific). Sections (10 µm) were cut using a NX50 CryoStar Cryostat (Thermo Scientific) and mounted on glass slides for immunostaining. For immunofluorescence, the cryosections were permeabilized with 0.5% v/v Triton™ X-100 (Millipore Sigma) in PBS for 30 min and blocked with 5% v/v normal chicken serum (NCS) in PBS for 1 h. We treated sections with TrueBlack® Lipofuscin Autofluorescence Quencher (Biotium, Fremont, CA) to reduce neurofibroma autofluorescence. Tissue sections were incubated with primary antibody diluted in 1.5% v/v NCS at 4 °C for 48 h. After three washes with PBS, coronal sections and secondary antibodies diluted in 1.5% v/v NCS were incubated for 1 h at RT. For staining of tdT and Sox10 we used chicken anti-mCherry (cat. MCHERRY-002; Aves Labs, Davis, CA) at a dilution of 1:200 and rabbit anti-SOX10 at a dilution of 1:100 (cat. no. AB227680; Abcam, Waltham, MA). Secondary antibodies (both at 1:350 working dilution) were goat anti-chicken Alexa594 and goat anti-rabbit-Alexa647 (both from ThermoFisher). For GFP immunostaining we used Chicken anti-GFP antibody (GFP1020, Aves Labs) at a dilution of 1:500.

Slides were cover slipped with Vectashield mounting medium with DAPI (Vector Laboratories, Burlingame, CA) and imaging was performed with a NIKON CSU-W1 spinning disk confocal microscope.

Candidate pooled barcoded library screen in adult mice. Three adult male C57BL/6 mice were intravenously injected with 7.0×10^{10} vg of the five pooled, barcoded capsids (1.4×10^{10} vg/capsid). Two weeks later, deeply anesthetized animals were perfused with cold PBS. We harvested sciatic nerves, brain, liver, and heart from each animal. Samples for DNA extraction were immediately frozen on dry ice and stored at −80 °C. This experiment was performed once.

DNA isolation from mice for barcoded AAV capsid candidates. Tissue samples (~ 25 mg) were homogenized using 1.4 mm ceramic beads in a BeadBug tissue homogenizer (Benchmark Scientific) in buffer ATL of the DNeasy Blood and Tissue Kit (Qiagen). After homogenization, we followed the manufacturer's instructions to purify DNA. DNA concentration was determined using a NanoDrop spectrophotometer (ThermoFisher Scientific).

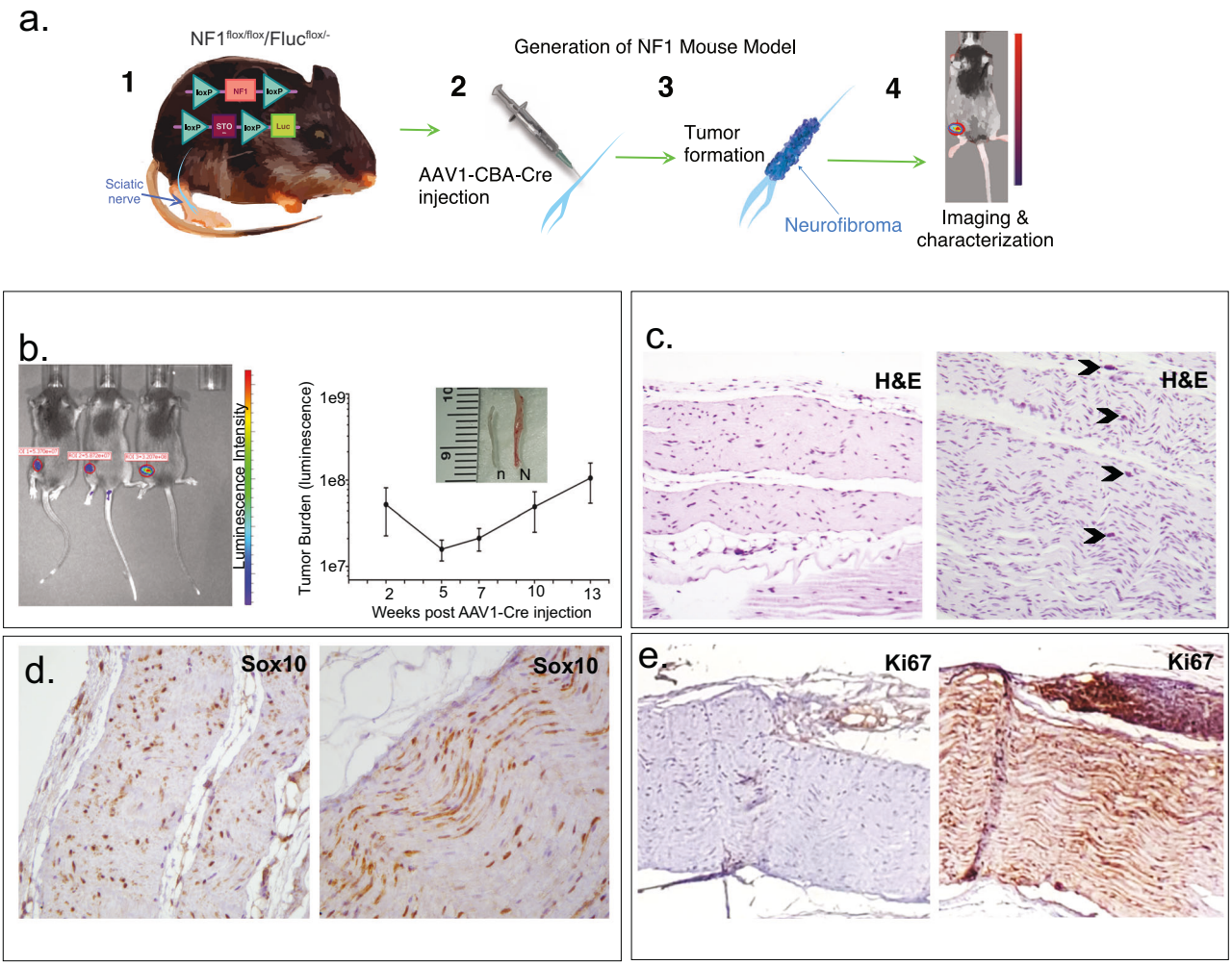

Fig. 1 NF1$^{flox/flox}$/Fluc^{flox} induced tumor mouse model and characterization of neurofibroma. a Overview of NF1 mouse model generation. Transgenic mice contain both NF1 floxed alleles and a floxed stop firefly luciferase (Fluc) cassette. AAV-Cre injection into the sciatic nerve induces neurofibroma formation which can be monitored by Fluc bioluminescence. **b** left image: In vivo bioluminescence imaging of neurofibroma showing Fluc activity detected on the left sciatic nerve indicating tumor formation. right graph: Increased Fluc activity seen on the sciatic nerve bearing neurofibroma corresponds to the tumor growth post-injection with AAV1-CBA-Cre vector ($n = 9$). Inset image: Compared to the contralateral naïve nerve, "n" (NF$^{+/+}$), the sciatic nerve bearing neurofibroma, "N" (NF$^{-/-}$), is markedly thickened and highly vascularized. **c** Hematoxylin & Eosin staining. Sagittal section of the naïve sciatic nerve (left image) and neurofibroma (right image). Sciatic nerve bearing neurofibroma demonstrated features of early neurofibroma such as hypercellularity and mast cells infiltration (arrows). **d** Comparing the sagittal section of the naïve sciatic nerve (left image), there are more Sox10-positive cells in the neurofibroma within the hypercellular area (right image). **e** At 14 weeks post-implantation, naïve sciatic nerve has no to minimal Ki67-positive cells (left image), whereas the sciatic nerve with neurofibroma shows marked Ki67 signal indicating high mitotic activity at the tumor site (right image).

PCR to amplify barcodes for NGS. A PCR using the DNeasy-purified DNA as template was performed (150 ng DNA template input). We used Q5 polymerase (NEB) and primers that amplify a 182 bp amplicon which contains the unique barcode for each capsid. Primers were: SC-Lib-Fwd (5′ GATGCTTACCCTTACGACGT 3′) and SC-Lib-Rev (5′ CAGCGTATCCACA-TAGCGTA 3′). The PCR product was purified using the QIAquick PCR purification kit (Qiagen) and samples were submitted for NGS as described above. We initially sequenced an aliquot of the pre-injected pooled barcoded AAV capsids to ascertain the precise frequencies of the barcoded variants on input. Output frequencies in all tissues were normalized to these initial ratios. Insert-containing sequence reads were binned using Hamming distance, comparing to the known barcode sequences; additional quality control was undertaken to ensure only true barcoded reads were assigned to each capsid.

Statistics. We used GraphPad Prism 10.3.1 for PC for statistical analysis. For comparison of AAV barcoded genome frequency between capsids and across tissues we used a 2-way ANOVA followed by a Dunnett's multiple comparisons test. For comparison of biodistribution or transduction of a single tissue between three capsids we used an Ordinary one-way ANOVA followed by a Dunnett's multiple comparisons test. For comparison of two capsids for biodistribution to or transduction of sciatic nerve we used an unpaired two-tailed t test. p values < 0.05 were accepted as significant.

RESULTS

Nf1$^{flox/flox}$/Fluc^{flox} induced mouse tumor model with characteristics of neurofibroma

We used Nf1-flox/flox (off) transgenic mice [19] crossed to Fluc-flox (on) mice [14]. We injected AAV1-CBA-Cre into the left sciatic nerve of young adult mice (total dosage of 6×10^{10} vg/mouse), such that Cre knocked out *Nf1* function, through the use of conditional (*Cre/lox*) alleles and turned on luciferase (which has a floxed STOP cassette) (Fig. 1a). This injection into the sciatic nerve could have produced minor injury to the nerve, with nerve injury being associated with NF1-null neurofibroma formation [20, 21]. The right sciatic nerve was not injected and termed the naïve nerve. Using in vivo bioluminescence imaging, firefly luciferase

(Fluc) activity was detected on the left sciatic nerve indicating tumor formation, beginning 2 weeks post-injection (Fig. 1b; $n = 9$). Five weeks post-injection, we observed increased tumor growth (increased luciferase activity) on the left sciatic nerve up to the 13th week post-injection. Naïve nerves and those bearing neurofibroma were harvested for further characterization. Gross anatomical assessment indicated that the tumor-bearing sciatic nerve (Nf1$^{-/-}$) was markedly thickened and highly vascularized as compared to the contralateral naïve nerve (Nf1$^{+/+}$; Fig. 1b, inset). Histopathological examination confirmed features of neurofibroma, such as hypercellularity, expansion of the nerve, presence of mast cells, mixed composition of SCs and fibroblasts, consistent with early neurofibroma formation (Fig. 1c). Immunohistochemical analysis showed that the neurofibroma had many SCs, as indicated by Sox10 immunoreactivity (Fig. 1d). Scattered proliferating cells highlighted by Ki67 expression are associated with a neurofibroma (Fig. 1e). Taken together, both the histological and molecular characteristics of the tumor from the AAV1-Cre injected sciatic nerve were consistent with those of neurofibroma.

In vivo selection in the neurofibroma model identified AAV capsids that traffic to the tumor after systemic injection

As previously described [11] AAV9 7-mer peptide-display library was produced by transfection of 293 T cells with the library plasmids. Before library production, the plasmid library was sequenced via next generation sequencing (NGS) and confirmed the presence of 21-mer inserts (coding for 7-mer peptides) and lack of variant bias. We then packaged the capsid library, performed NGS and confirmed that the vector creation process maintained sufficient diversity (based on experience with prior successful selections [11, 17]).

To perform the selection, we injected the Nf1$^{flox/flox}$/Fluc^{flox} neurofibroma-bearing mice ($n = 2$) with the AAV peptide library via tail vein i.v. injection at a dosage of 4×10^{10} vg/mouse. Two consecutive rounds of selection were performed, with the composition of the viral pool assessed at each round by next generation sequencing (NGS) (Fig. 2a). Two weeks post-injection, the sciatic nerve with neurofibroma and its equivalent contralateral side (naïve nerve) were harvested for DNA isolation and purification. We recovered cap gene sequences via PCR from both neurofibromas and one of the naïve nerves. We found numerous 7-mer variants were enriched in sciatic nerves. We then pooled the PCR amplified cap gene containing the inserts extracted from the neurofibroma samples and cloned them into the AAV plasmid backbone to produce vector for round two.

For the second round of selection, we injected two Nf1$^{flox/flox}$/Fluc^{flox} neurofibroma-bearing mice with the library generated from round 1 at a dose of 1.15×10^{10} vg/mouse, via the tail vein. Two weeks post-injection, the animals were euthanized, and sciatic nerves were harvested. We recovered variants from both neurofibromas ($n = 2$) and naïve nerve ($n = 2$) and subjected the resulting PCR amplicons separately for NGS. Peptide sequences encoded by the 21-mer inserts in cap for each of the four samples are shown (Fig. 2b). We compared the profile from each nerve/neurofibroma and chose one variant, RPDHLPP (called AAV-SC3) to test further as it was found at similar frequency (3.4 to 4.3%) in both mice in the neurofibroma, but not the naïve sciatic nerve (Fig. 2b).

AAV-SC3 transduces neurofibroma after systemic injection of mice

To ascertain if AAV-SC3 had higher efficiency at neurofibroma targeting than the parental AAV9 capsid, we constructed an AAV expression plasmid which encodes tdT under the rat P0 promoter. This promoter was used to restrict expression to SCs for two main reasons. First, it allows more specific expressing thus preventing confounding results in quantitative PCR and imaging assays, such as transduced neurons and their axons in the sciatic nerve. Second, using the P0 promoter should be safer than a more ubiquitous promoter when developing a therapeutic to treat neurofibroma. Expressing the transgene in target (SCs) vs non-target cells (e.g. liver) may prevent off-target toxicity observed with transgene overexpression [22]. The AAV construct is shown in Fig. 3a. We also included another capsid, AAV-F, which was originally identified by its high efficiency of crossing the blood-brain barrier in mice [11, 23, 24] and subsequently we observed transduction of sciatic nerve after intrathecal injection in non-human primates [25].

Nf1$^{flox/flox}$/Fluc^{flox} mice were injected in both sciatic nerves with 10^{10} vg of AAV1-Cre to induce two neurofibromas/mouse. After 34 days, mice ($n = 5$/group) received systemic injections of 10^{12} vg of AAV9-P0-tdT, AAV-F-P0-tdT, or AAV-SC3--P0-tdT and 6 weeks later tissues were harvested. From each mouse, one neurofibroma was used to quantitate tdT expression at the mRNA level by RT-ddPCR and the other was post-fixed in formaldehyde, cryoprotected, and sectioned for immunofluorescence analysis. We also analyzed the biodistribution of each capsid's packaged genomes in brain and liver using qPCR with specific probes and primers to detect the tdT DNA. We observed that one of the animals injected with AAV-SC3 had a 100-fold decrease in vgs compared to all other mice in the group (data not shown). This likely indicated a failed tail vein injection and this animal was excluded from further analysis. As expected from prior studies [11, 26], AAV-F displayed a significant increase ($p = 0.008$) of 45-fold compared to AAV9 at biodistribution to brain (Fig. 3b). In contrast AAV-SC3 displayed a similar (non-significant) biodistribution to brain compared to AAV9 (Fig. 3b). Means for vector genomes in liver were not significantly different between any of the groups (Fig. 3b).

Next, we analyzed the levels of tdT mRNA in one neurofibroma per mouse to assess transgene expression mediated by each capsid. RNA was isolated, treated with DNase I to remove residual AAV genomes, and RT-ddPCR performed to quantify cDNA levels compared to a reference cDNA for PPIA. Interestingly with AAV-SC3, we found a 2.1-fold increase ($p = 0.111$) and 6.5-fold ($p = 0.008$) increase in tdT cDNA levels over AAV9 and AAV-F, respectively (Fig. 3c). There was no significant difference of tdT cDNA levels between AAV9 and AAV-F.

To confirm expression of tdT in the neurofibroma, we immunostained sciatic nerve cryosections with an antibody against tdT and fluorescence was measured using confocal microscopy. No specific tdT immunostaining was detected in the no vector (control) mouse neurofibroma as expected (Fig. 3d). For both AAV9 and AAV-SC3 i.v. injected mice, we detected scattered transduction of cells with distinct SC cell morphology (Fig. 3d). We also detected transduction of cells with AAV-F, but the labeling was qualitatively less frequent than AAV9 and AAV-SC3, which corroborated the RT-ddPCR data (Fig. 3d). To confirm that AAV9 and AAV-SC3 were mediating transgene expression in SCs within the neurofibroma, tissue sections were immunostained for both Sox10 as well as tdT. We detected transduced, tdT immunostained cells with Sox10-positive nuclei for both capsids, indicating transduced SCs (Fig. 3e).

AAV-SC3 and AAV9 transduce normal nerve in mice after systemic injection

To test if AAV-SC3 can transduce naïve nerve, we injected adult male C57BL/6 mice with 10^{12} vg ($\sim 4 \times 10^{13}$ vg/kg) of either AAV-SC3-P0-tdT or AAV9-P0-tdT. Seven weeks post-injection, tissues were harvested, and DNA extracted from liver and sciatic nerves (Fig. S1a). AAV-SC3 had slight, 1.4-fold, higher AAV genomes in sciatic nerve compared to AAV9, although this did not reach statistical significance (Fig. S1b). AAV genomes in liver were much higher for both groups than in sciatic nerves, 120-fold higher for AAV-SC3 and 331-fold higher for AAV9, respectively (Fig. S1b). Interestingly, there was a small, 1.9-fold, yet statistically significant decrease in AAV genomes in the liver with AAV-CAP.NF compared

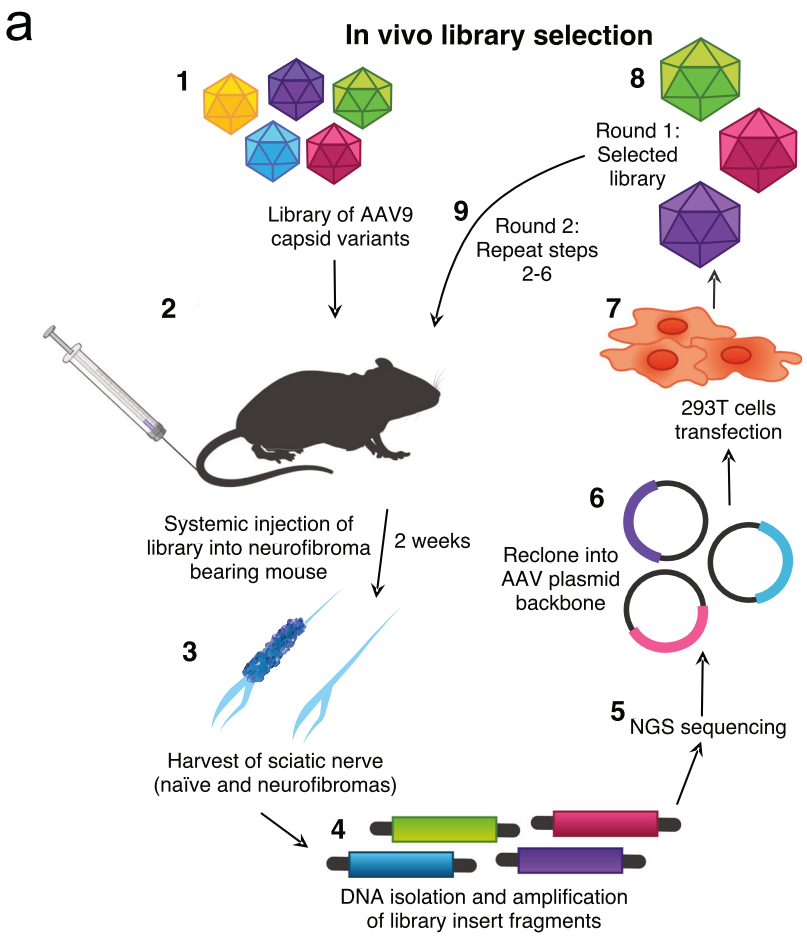

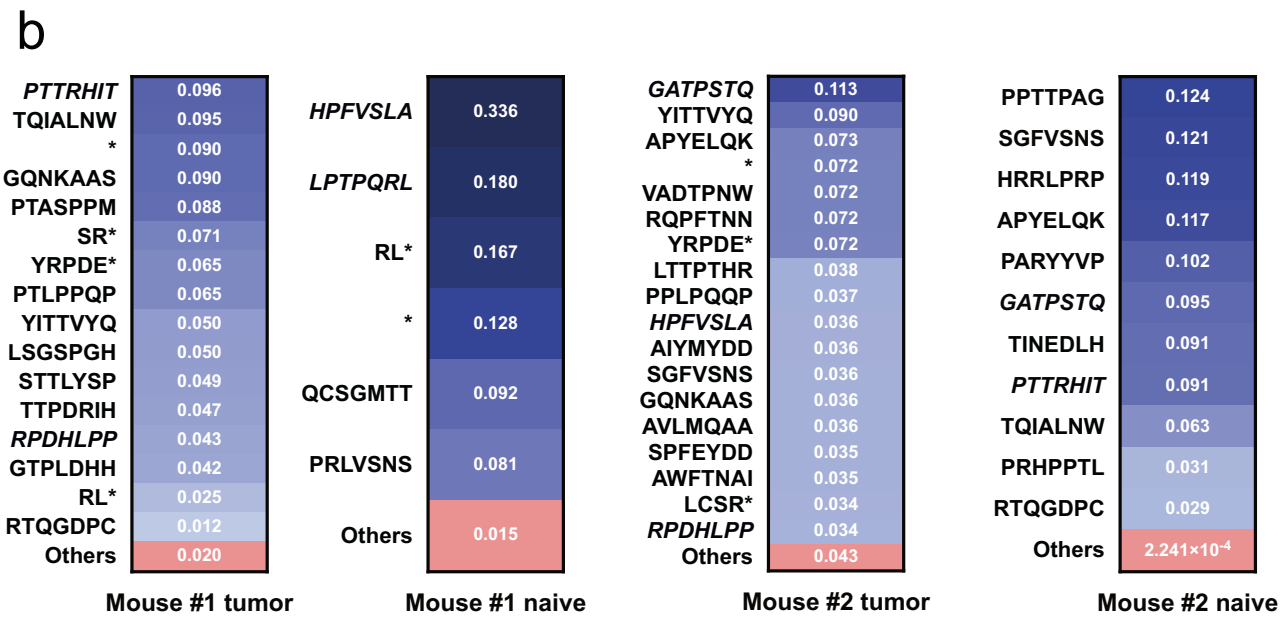

Fig. 2 In vivo selection with an AAV peptide display library allows enrichment of variants recovered from the second round in the sciatic nerve of Nf1$^{flox/flox}$/Fluc^{flox} induced tumor model. a In vivo library two-round selection scheme to isolate AAV capsid variants that transduce neurofibroma. **b** Round two next generation sequencing (NGS) results of AAV peptide inserts isolated from the neurofibroma (tumor) and naïve (no tumor) nerve. Each chart show enrichment after second round of library selection, with darker blue shading representing higher read frequency. The red chart region represents all of the other sequence variants.

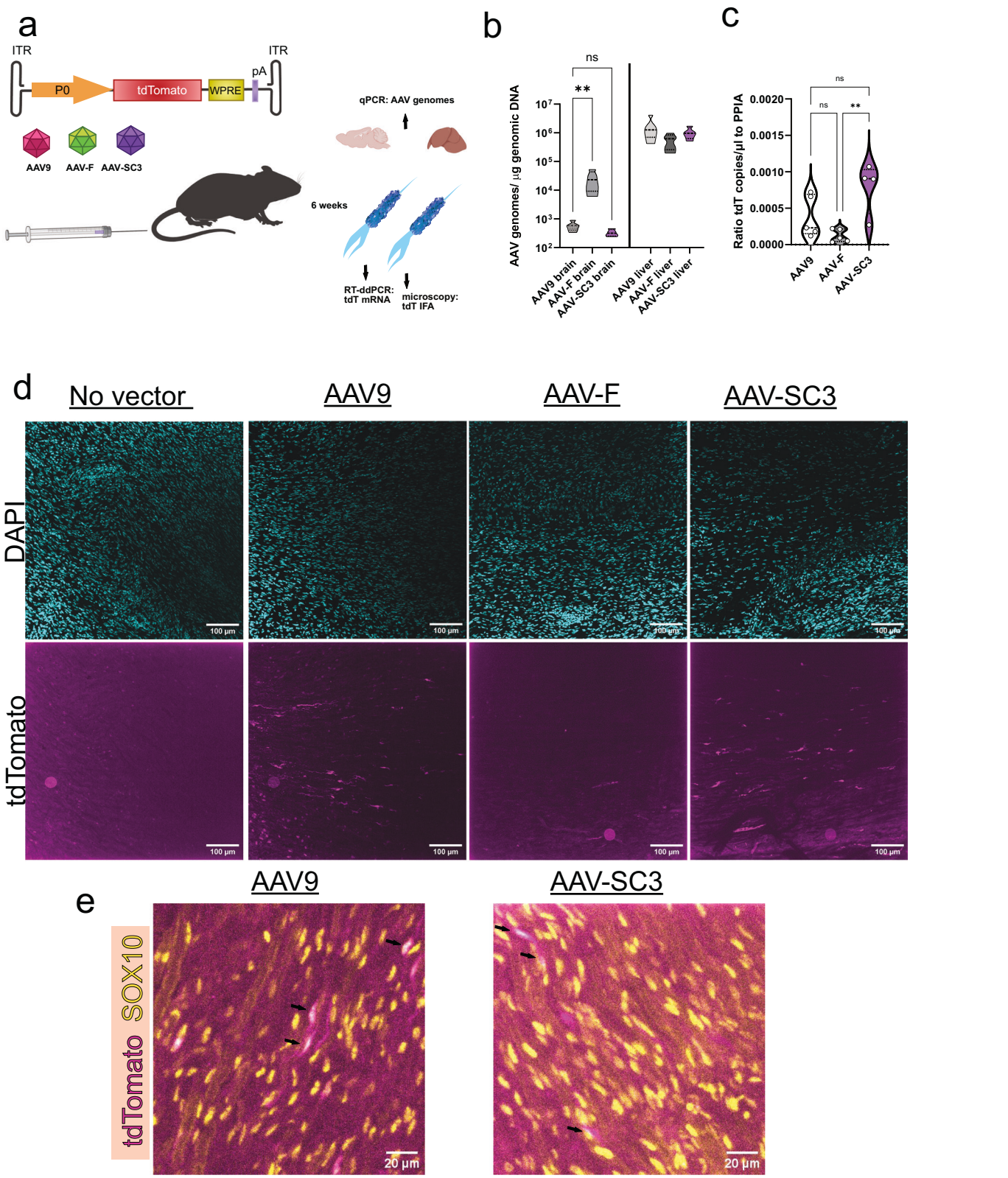

to AAV9. To assess whether the biodistribution of AAV-SC3 was more selective for sciatic nerve vs. AAV9 we calculated the sciatic nerve/liver AAV genome ratio for each animal. We observed a significant, 3.2-fold increase in selectivity of AAV-SC3 compared to AAV9 for sciatic nerve (Fig. S1c). Next, we measured the transduction of sciatic nerve using RT-ddPCR of tdT cDNA. There was a slight, non-significant, 1.5-fold increase in tdT cDNA levels for AAV-SC3 compared to AAV9 (Fig. S1d). In liver, the amount of tdT cDNA levels were much higher, tracking with the AAV genome levels and there was a small, non-significant, 1.09-fold increase

Fig. 3 AAV-SC3 displays similar biodistribution to liver and brain as AAV9, but increased transgene expression in sciatic nerve of neurofibroma-bearing mice. a An AAV expression cassette was constructed with a rat PO promoter driving tdT cDNA expression. $Nf1^{flox/flox}$/$Fluc^{flox}$ mice had neurofibroma induced in both sciatic nerves with local AAV1-Cre injection. After neurofibroma formation, mice were injected i.v. with three groups of capsids packaging the expression cassette. Six weeks post-injection both neurofibroma were harvested as well as brain and liver for molecular and histological analysis. ITR, inverted terminal repeat; WPRE, woodchuck hepatitis virus post-transcriptional regulatory element; pA, polyadenylation signal. **b** Biodistribution of AAV genomes in brain and liver. $^{**}p = 0.008$. **c** RT-ddPCR quantitation of tdT mRNA in whole neurofibroma-bearing nerves from each group of mice. ns=not significant; $^{**}p = 0.008$. **d** Immunofluorescence detection of tdT expression in neurofibroma of mice injected with AAV vectors. Specific labeling of anti-tdT immunostained cells of SC morphology were observed in the injected mice, most frequently in the AAV9 and AAV-SC3 injected groups. Scale bar=100 µm. DAPI=blue; tdT immunofluorescence=magenta. **e** AAV9 and AAV-SC3 can both transduce SCs in neurofibroma. Sections were immunostained for transgene expression (tdT, magenta) and Sox10 (yellow). Co-localized cells are shown in white and indicated by black arrows. For (**b**) and (**c**), AAV9, $n = 5$; AAV-F, $n = 5$; AAV-CAP.NF, $n = 4$ For d**.:** AAV-9, $n = 4$; AAV-F, $n = 5$; AAV-SC3, $n = 4$.

Table 1. Candidates for further screening for biodistribution to sciatic nerve.

Variant	AA sequence	% of total reads	In vivo characteristics
AAV-SC1	STTLYSP	4%	Found in mouse 1 tumor
AAV-SC2	LPTPQRL	18%	A top clone in naïve nerve
AAV-SC3	RPDHLPP	3–4%	Similar levels in both neurofibromas
AAV-SC4	GATPSTQ	9–11%	A top clone in nerves with and without neurofibromas

with AAV-SC3 compared to AAV9 (Fig. S1e). To assess the cellular localization of transduction, we performed confocal microscopy on immunostained sections of liver and sciatic nerve of representative animals from both vector groups and the control group (no vector). In liver, intense tdT immunofluorescence was observed in cells with hepatocyte morphology for both capsids (Fig. S1f). In sciatic nerve we stained for both tdT and Sox10 to assess transduction of SCs. For both capsids, there were only a few detectable tdT+ Sox10 -positive SCs within each examined section (Fig. S1g). Overall, this shows that while the biodistribution of AAV genomes has been significantly shifted for AAV-SC3 vs AAV9, the transgene expression has not.

Identification of an AAV capsid variant displaying a putative laminin binding peptide with enhanced biodistribution to sciatic nerve after systemic injection

While direct transduction of neurofibroma with AAV could be potentially useful for control of established tumors, their heterogeneous cellular composition and relatively fast cell turnover makes this a difficult challenge. Identifying capsids which could mediate gene delivery to SCs of peripheral nerves could also be useful for prophylactic treatment before neurofibroma initiation (or for other diseases that affect SCs). Since in our selection we isolated capsids from both neurofibromas and naïve nerve (Fig. 2b), we selected four candidates, AAV-SC1-4 (Table 1) for further testing for naïve nerve biodistribution. We attempted to include the most frequent variant, HPFVSLA, but vector yield for this capsid was too low for in vivo use (data not shown). Each of the four capsids were cloned into conventional rep/cap plasmids and vectors packaged an AAV expression cassette with unique barcodes for each capsid. For benchmarking purposes, we also included an AAV9 capsid also packaging a unique barcoded expression cassette. All five capsids were pooled in an equal ratio and a total of 7×10^{10} vg/mouse (1.4×10^{10} vg/capsid/mouse) were injected into $n = 3$ adult male C57Bl/6 mice. Two weeks later, we harvested sciatic nerves, liver, brain, and heart and isolated AAV genomes (Fig. 4a). For each tissue, the barcode inserts were amplified using PCR and NGS performed to determine the profile of each capsid. Of all the capsids, only AAV-SC4 showed an average of ~5-fold (and up to 7-fold) significant increase in sciatic nerve (Fig. 4b, c). Interestingly AAV-SC4 appears to be more selective to sciatic nerve over other tissues such as brain, heart, and liver which were not significantly increased over AAV9 (Fig. 4c). A database search revealed that the STQ peptide, contained in the GATPSTQ 7-mer, is a known laminin binding peptide [27]. Laminins are glycoproteins of the extracellular matrix and critical for SC function [28].

To assess whether AAV-SC4's increased biodistribution resulted in enhanced transduction of SCs, we compared a direct, dose-matched comparison to AAV9, both packaging the AAV-P0-tdT expression cassette. For each capsid, six C57Bl/6 mice (3 males, 3 females) were injected intravenously with 10^{12} vector genomes/mouse. Seven weeks post injection, mice were euthanized and sciatic nerves harvested (Fig. 5a). One nerve was utilized for isolation of AAV genomes and tdTomato qPCR. We observed a significant ($p = 0.0027$), 6.3-fold increase in AAV genomes in sciatic nerve with AAV-SC4 compared to AAV9 (Fig. 5b). When mice were grouped based on vector type and sex, we noticed that AAV9 in female mice trended towards higher biodistribution than AAV9 in male mice, while AAV-SC4 biodistribution was more consistent between sexes (Fig. 5c). However, this did not achieve statistical significance. We measured tdT mRNA levels using RT-ddPCR. Unexpectedly, the average tdT cDNA was higher by 1.73-fold for AAV9 compared to AAV-SC4, however there was a large variability between mice in the AAV9 group (Fig. 5d). To confirm the tdTomato cDNA expression data, we assessed transduction of SCs in sciatic nerve by immunostaining for tdTomato and SOX10. For AAV9, similar to prior experiments, we observed sporadic tdTomato positive cells within the nerve, with even fewer transduced cells observed for AAV-SC4 (data not shown), which aligned with the RT-ddPCR data. We wondered if AAV-SC4 might transduce other cell types in the sciatic nerve, with the P0 promoter preventing efficient tdTomato mRNA transcription in those other cells. To evaluate this, we packaged a self-complementary (sc) AAV genome which contained a strong chicken beta actin (CBA) promoter driving GFP inside AAV-SC4 (Fig. 6a). Adult C57Bl/6 mice were injected systemically with 1×10^{11} vg ($\sim 4 \times 10^{12}$ vg/kg) of AAV-SC4-CAG-GFP and three weeks post injection sciatic nerves and livers were harvested for immunofluorescence analysis of GFP expression. We assessed transduction of liver which is generally highly transduced by AAV vectors. Robust transduction of liver was detected for the three injected mice (Fig. 6b). This confirmed that AAV-SC4 was competent at transduction of cells in vivo. Next, we assessed transduction of sciatic nerves in the three injected mice by immunostaining for GFP as well as Sox10 to mark SCs. We observed GFP positive immunostaining throughout the nerves in each mouse, in contrast to the control nerve from mice not injected with vector (Fig. 6c). While some of the GFP immunoreactivity appeared to be inside axons (no DAPI colocalization), we

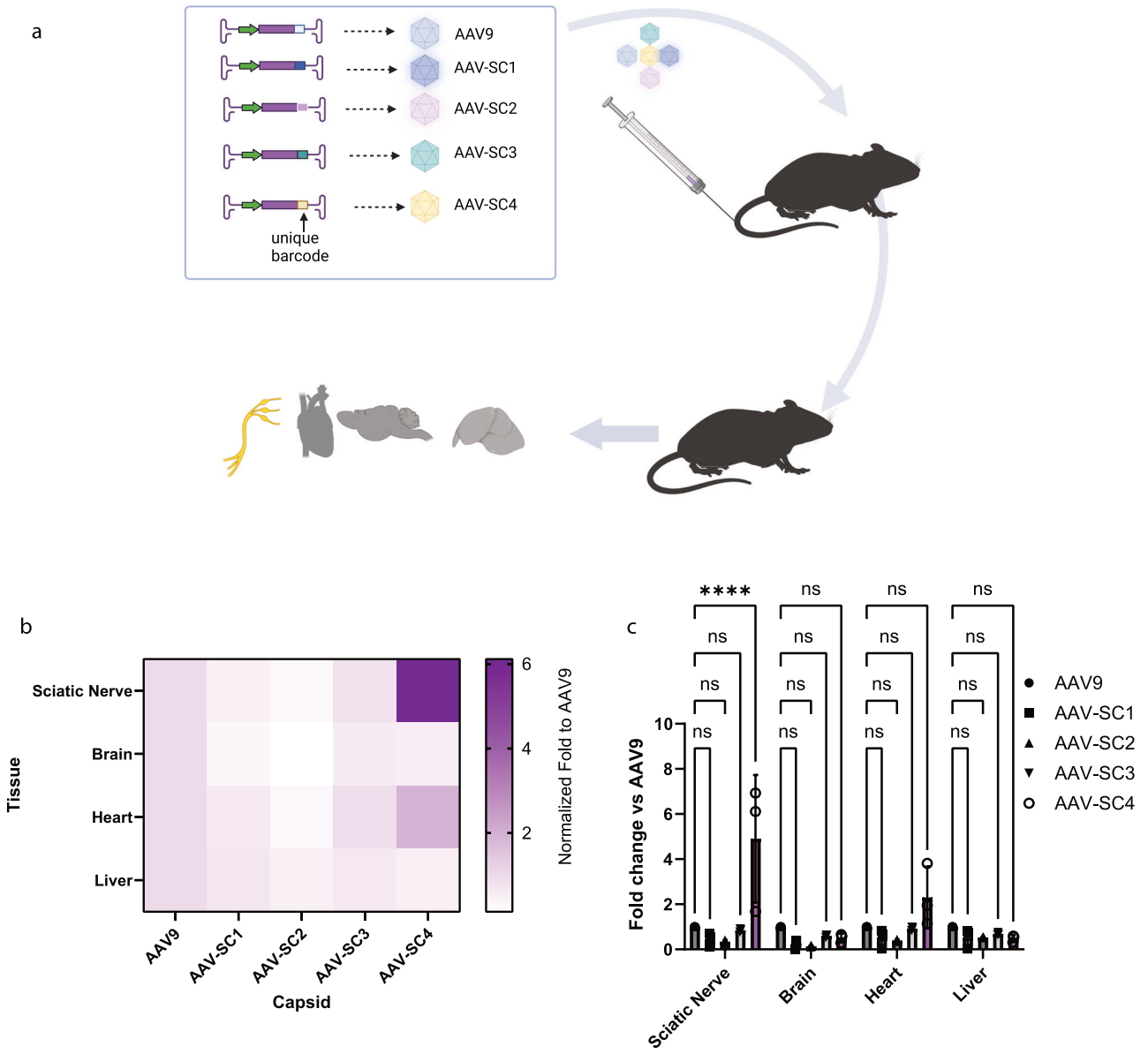

Fig. 4 Identification of an AAV capsid variant with enhanced biodistribution to sciatic nerve after systemic injection. a Schematic of experiment. Four capsids from the in vivo selection, SC1-4, as well as AAV9, were produced, each packaging a uniquely barcoded genome. The pooled capsids were injected systemically into C57Bl/6 mice and two weeks later sciatic nerve and other tissues harvested and barcode read frequency determined using NGS of the amplified AAV genomes. **b** Heat map of read frequency for each capsid variant normalized to AAV9 reads for each tissue. **c** Graph of fold-change for each capsid across different tissues. ns not significant; ***$p < 0.001$.

observed strong colocalization of GFP with SOX10, which indicates AAV-SC4 can transduce SCs after systemic delivery in mice (Fig. 6c, d).

DISCUSSION

While others have tested AAV's for transduction of peripheral nerves in mice [7], to our knowledge this is the first study to test different AAV vectors injected systemically for gene delivery to an in vivo model of NF1. As part of this study, we developed a novel nerve-associated NF1 mouse neurofibroma model which produced focal neurofibroma in the sciatic nerve after injection of AAV1-Cre into young adult $Nf1^{flox/flox}$/$Fluc^{flox}$ mice, so that the presence and size of tumors could be monitored by in vivo bioluminescence imaging. This model is similar to that of Dodd et al. [29], who injected adenovirus-Cre into the sciatic nerve of $Nf1^{flox/flox}$ mice. In our case, bioluminescent tumors appeared within 3–8 weeks, which were deemed to resemble early neurofibroma in NF1 patients using H&E neuropathology and IHC for the SC marker, Sox10 and proliferation marker, Ki67 [30]. This neurofibroma model was used together with an AAV9 peptide display library to identify a novel capsid variant, AAV-SC3, which mediates transduction of neurofibroma in mice after systemic delivery. Compared to the parental capsid, AAV9, we observed enhanced transduction of neurofibroma (2.1-fold) after systemic injection in mice. We used the P0 promoter based on earlier work as it drives selective expression in SCs. While this did not achieve statistical significance ($p = 0.111$) at the group sizes tested ($n = 4$–5 mice), it did provide promising proof of concept data that AAV capsid engineering and in vivo selections can lead

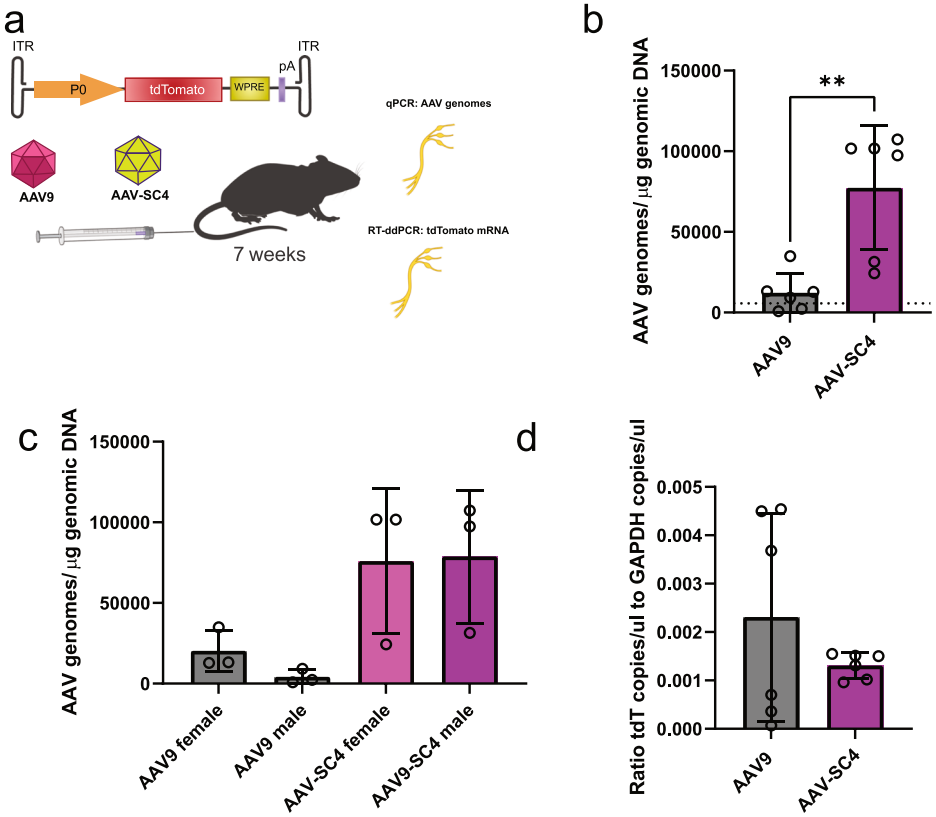

Fig. 5 Side by side comparison of AAV9 and AAV-SC4 biodistribution to and transduction of sciatic nerve in C57BL/6 mice after systemic administration. a AAV9 or AAV-SC4 vectors packaging AAV-P0-tdTomato were injected systemically into male ($n = 3$) and female ($n = 3$) C57BL/6 mice (total $n = 6$/vector group). Seven weeks later, sciatic nerves were harvested to quantitate AAV genomes and tdTomato expression. **b** AAV genome quantitation in sciatic nerve. Each data point represents an individual mouse. The dotted line indicates qPCR values from control mice not treated with vector. $^{**}p = 0.0027$. **c** Data in (**b**) separated by mouse sex. **d** RT-ddPCR quantitation of tdT mRNA in whole neurofibroma nerves from each group of mice.

to transduction of neurofibroma. We chose AAV-SC3 (peptide RPDHLPP) as it was represented in the top sequencing reads in two mouse neurofibromas (Fig. 2). We also performed a screen of four chosen candidate capsids from round two of the selection (AAV-SC1–4). This selection included AAV-SC3 as well as AAV9 for benchmarking the new capsids. The goal of the screen was to identify capsids that distribute to the normal sciatic nerve after systemic injection in healthy mice. Through this selection we identified a new capsid, AAV-SC4, which mediated 6-fold enhanced biodistribution to sciatic nerve compared to AAV9. Interestingly, we did not observe a significant increase in P0 promoter-driven transgene expression of AAV-SC4 over AAV9, which made us question whether the capsid was functional at transduction. To test this we packaged a self-complementary AAV-CBA-GFP expression cassette into AAV-SC4.The broadly active CBA promoter was chosen to assess a wider array of cell types in the nerve, as the P0 promoter has higher activity in myelinating SCs (MSCs) vs non-myelinating SCs (NMCs) [31]. Using this promoter, we observed that AAV-SC4 mediated transduction of cells throughout the sciatic nerve, confirming the capsid's transduction capability. We performed confocal microscopy using staining for GFP and SOX10 to understand whether MSCs and or NMSCs were transduced by AAV-SC4. We found colocalization of some of the GFP positive cells with SOX10-positive cells, which indicates that AAV-SC4 can indeed transduce SCs. Future work will determine the specific SC type(s) AAV-SC4 is transducing and in comparison to AAV9. This result also indicates that the P0 promoter (at least the version we utilized) may not always be the best option for transgene expression in SCs, particularly those with lower activity of this promoter. Another explanation for the lack of apparent P0 promoter activity with SC4 in contrast to SC3 and AAV9 could be due to differences of this capsid recruiting transcriptional machinery to the this promoter in the AAV genome as described [32–34]. Since the CBA promoter does seem to be active in SCs (Fig. 6) in future construct designs detargeting expression from neurons may be achieved using miRNA-based expression detargeting as has been done to increase transduction selectivity for microglia [35].

AAV-SC4 contains a well described laminin binding motif, STQ. Schwann cells and neurofibroma both display laminin localized primarily to the basement membrane [36].One study identified STQ-motif containing peptides that selectively bound denatured laminin using bacteriophage peptide display [27]. The identified STQ peptide was found to reduce tumor cell migration, angiogenesis, and metastasis [27] in mice. In another independent study, phage display identified an STQ-containing peptide that bound to the vesicular stomatitis virus glycoprotein (VSV-G) on lentiviruses and this allowed increased lentivirus transduction of HT1080 cells [37]. While we did not intentionally target laminin using our in vivo selection strategy, the identification of an amino acid motif with a known ligand for peripheral nerve/neurofibroma may be useful for further improving AAV and other delivery modalities (e.g. extracellular vesicles, lipid nanoparticles, etc.). In future experiments, we will test other routes of administration of AAV-SC4 via intrathecal or direct intra-nerve injection. We will also test AAV-SC4 for transduction of neurofibroma, as the AAV-SC4 peptide was detected in both neurofibroma and normal nerve in round two of selection (Fig. 2b). Finally, enhanced capsids may be

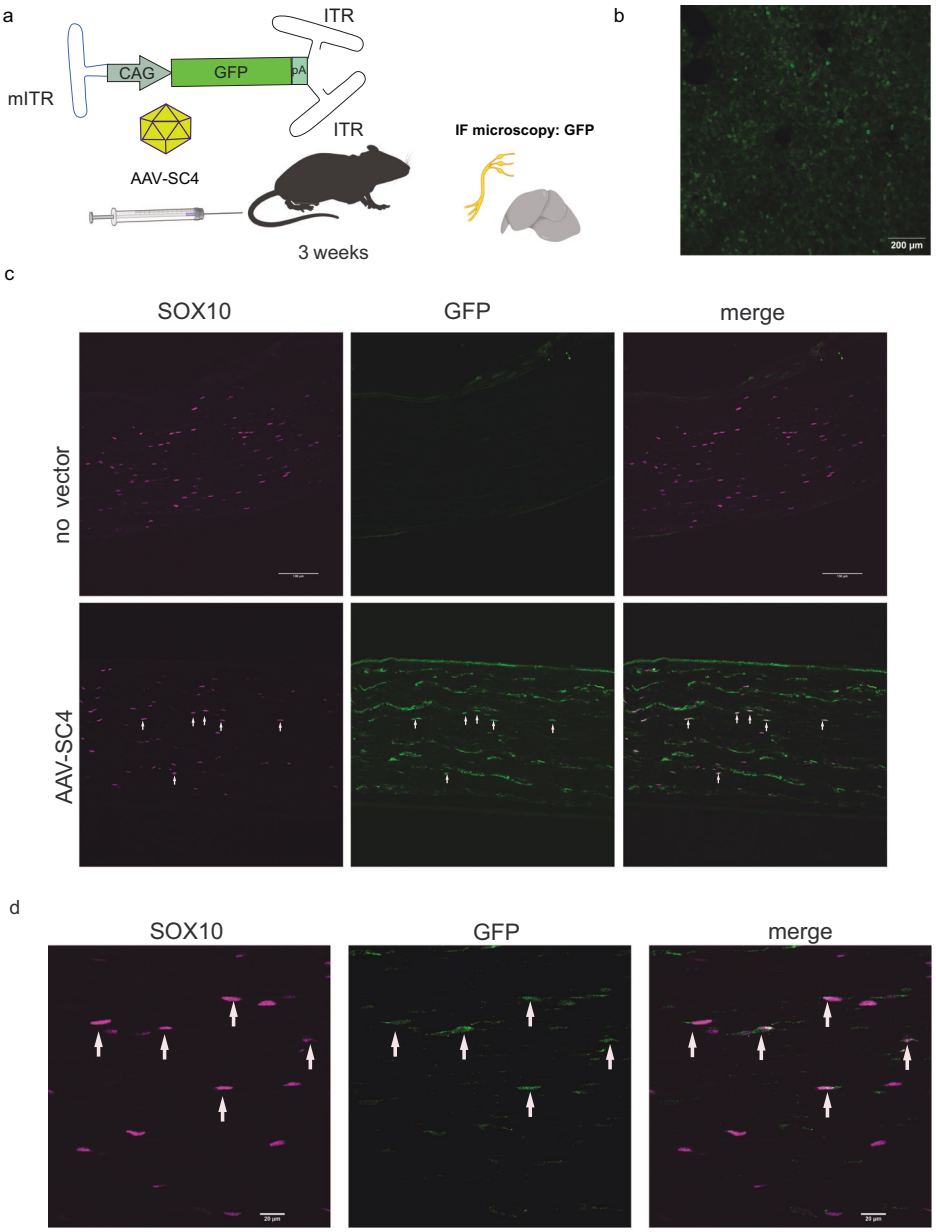

Fig. 6 AAV-SC4 capsid packaging a self-complementary (sc) AAV-CAG-GFP genome transduces sciatic nerve after systemic injection. **a** Overview of experiment. AAV-SC4 packaged a sc AAV-CAG-GFP expression cassette. mITR, mutated ITR. Tail vein injection of the vector into C57BL/6 mice and 3 weeks later, liver and sciatic nerve were harvested for immunofluorescence analysis. **b** Liver is highly transduced by AAV-SC4-scCAG-GFP. Scale bar= 200 µm. **c** Representative nerve of control, no vector mouse, and AAV-SC4 injected mouse. Scale bar= 100 µm. **d** High magnification image of a nerve from a AAV-SC4 injected mouse. Scale bar= 20 µm. In c and d, magenta= SOX10 immunostaining; green= GFP immunostaining. Arrows point to co-localized GFP/SOX10 immunostaining which indicates transduced Schwann cells.

engineered by affinity maturation of amino acids surrounding the STQ motif as previously demonstrated for other capsids [38].

Several studies have tested existing AAV serotypes for transduction of SCs after various routes of injection as mentioned in the Introduction. A recent study used an AAV peptide display library to identify AAV capsids that could transduce primary human SCs in culture [39]. These peptides Pep2hSC1 and Pep2hSC2 were inserted within the AAV2 capsid. The authors showed that these capsids could transduce human and rodent SCs, human plexiform neurofibroma cells as well as human nerve segments upon direct injection ex vivo. Interestingly, they observed better transduction efficiency in "healthy" SCs than NF1 patient-derived SCs, which may be due to the selection method based on healthy patient SCs. Finally, they achieved transduction of SCs in a nerve crush model in mice after direct intra-nerve injection. Both the AAV2-based Pep2hSC capsids as well as our AAV-SC3 and AAV-SC4 capsid may serve complementary roles in NF1/SC research. The AAV2-Pep2hSC capsids are well suited for in vitro transductions of human and murine NF1 cells and direct injection of nerve segments. The AAV-SC3 capsid, derived from AAV9, is suitable for systemic injections in mouse models of NF1 when broad biodistribution and potentially blood-brain barrier (BBB) penetration is desired (AAV9 has broader biodistribution and ability to cross BBB in contrast to AAV2 [40]). We found that AAV-SC3 had a similar biodistribution in the brain as compared to AAV9, thus, its inherent ability to cross the BBB

does not seem to be compromised by the peptide insert. This is important as neurofibroma can affect the central nervous system (CNS), as well as peripheral nervous system (PNS) [41] Finally, AAV-SC4 may be useful for transduction of peripheral nerves in mice as prophylactic strategies for NF1, and it should also be tested in models of NF1 and diseases of peripheral nerves.

AAV vectors, like other viruses and nanoparticles have a propensity to be biodistributed to the liver. Unless the liver is the target of therapy, this is generally undesirable as AAV transduction of liver has been associated with toxicity in both NHP studies and clinical trials [42, 43]. In this study, we assessed biodistribution to and transduction of liver after systemic injection of AAV9 or AAV-SC3 both packaging the AAV-P0-tdT expression cassette. For both vectors, high levels of both biodistribution and transgene expression (assessed by RT-ddPCR and microscopy) to liver were observed. There was a small decrease in biodistribution to liver by AAV-SC3 compared to AAV9, but this is likely insufficient. It was also apparent that at the high doses of vector genomes observed in liver, the selectivity of the P0 promoter was lost, as robust expression in hepatocytes was evident by confocal microscopy. Thus, in future development of AAV capsids for sciatic nerve transduction after systemic injection, detargeting from the liver at the steps of both biodistribution and transduction should be addressed. For reducing off target expression in liver with SC-targeted AAV's, incorporation of miRNA binding sites, such as those for miR122, have been successfully used by others [44, 45]. Using these two strategies may increase the on-target biodistribution to SCs as well as reduce off target expression.

Overall, our work provides a new semi-quantitative model of NF1 neurofibroma in mice and important conceptual data that AAV selection approaches can be used for neurofibroma transduction in vivo. AAV-SC3 and AAV-SC4 should be useful for testing new gene therapy approaches in mouse models of NF1 as well as other models of peripheral nerve diseases.

DATA AVAILABILITY

Data are available upon request. Plasmid expressing the capsid gene for AAV-SC4 is available at Addgene (Plasmid ID 236254).

CODE AVAILABILITY

All code written and used in this study can be accessed by emailing the authors, who will provide scripts and methods of use.

REFERENCES

1. Mendell JR, Al-Zaidy SA, Rodino-Klapac LR, Goodspeed K, Gray SJ, Kay CN, et al. Current clinical applications of in vivo gene therapy with AAVs. Mol Ther. 2021;29:464–88.
2. Keeler AM, Flotte TR. Recombinant adeno-associated virus gene therapy in light of luxturna (and zolgensma and glybera): where are we, and how did we get here? Annu Rev Virol. 2019;6:601–21.
3. Ozelo MC, Mahlangu J, Pasi KJ, Giermasz A, Leavitt AD, Laffan M, et al. Valoctocogene roxaparvovec gene therapy for hemophilia A. N. Engl J Med. 2022;386:1013–25.
4. Pipe SW, Leebeek FWG, Recht M, Key NS, Castaman G, Miesbach W, et al. Gene therapy with etranacogene dezaparvovec for hemophilia B. N. Engl J Med. 2023;388:706–18.
5. Tai CH, Lee NC, Chien YH, Byrne BJ, Muramatsu SI, Tseng SH, et al. Long-term efficacy and safety of eladocagene exuparvovec in patients with AADC deficiency. Mol Ther. 2022;30:509–18.
6. Mendell JR, Sahenk Z, Lehman K, Nease C, Lowes LP, Miller NF, et al. Assessment of systemic delivery of rAAVrh74.MHCK7.micro-dystrophin in children with duchenne muscular dystrophy: a nonrandomized controlled trial. JAMA Neurol. 2020;77:1122–31.
7. Kagiava A, Richter J, Tryfonos C, Leal-Julia M, Sargiannidou I, Christodoulou C, et al. Efficacy of AAV serotypes to target Schwann cells after intrathecal and intravenous delivery. Sci Rep. 2021;11:23358.
8. Kagiava A, Karaiskos C, Richter J, Tryfonos C, Jennings MJ, Heslegrave AJ, et al. AAV9-mediated Schwann cell-targeted gene therapy rescues a model of demyelinating neuropathy. Gene Ther. 2021;28:659–75.
9. Tanguy Y, Biferi MG, Besse A, Astord S, Cohen-Tannoudji M, Marais T, et al. Systemic AAVrh10 provides higher transgene expression than AAV9 in the brain and the spinal cord of neonatal mice. Front Mol Neurosci. 2015;8:36.
10. Homs J, Ariza L, Pages G, Udina E, Navarro X, Chillon M, et al. Schwann cell targeting via intrasciatic injection of AAV8 as gene therapy strategy for peripheral nerve regeneration. Gene Ther. 2011;18:622–30.
11. Hanlon KS, Meltzer JC, Buzhdygan T, Cheng MJ, Sena-Esteves M, Bennett RE, et al. Selection of an Efficient AAV Vector for Robust CNS Transgene Expression. Mol Ther Methods Clin Dev. 2019;15:320–32.
12. Ortonne N, Carroll SL, Rodriguez FJ, Miller DC, Nazarian RM, Blakeley JO, et al. Assessing interobserver variability and accuracy in the histological diagnosis and classification of cutaneous neurofibromass. Neurooncol Adv. 2020;2:i117–i23.
13. Zhu Y, Ghosh P, Charnay P, Burns DK, Parada LF. Neurofibromas in NF1: Schwann cell origin and role of tumor environment. Science. 2002;296:920–2.
14. Woolfenden S, Zhu H, Charest A. A Cre/LoxP conditional luciferase reporter transgenic mouse for bioluminescence monitoring of tumorigenesis. Genesis. 2009;47:659–66.
15. Prabhakar S, Taherian M, Gianni D, Conlon TJ, Fulci G, Brockmann J, et al. Regression of schwannomas induced by adeno-associated virus-mediated delivery of caspase-1. Hum Gene Ther. 2013;24:152–62.
16. Ivanchenko MV, Hanlon KS, Devine MK, Tenneson K, Emond F, Lafond JF, et al. Preclinical testing of AAV9-PHP.B for transgene expression in the non-human primate cochlea. Hear Res. 2020;394:107930.
17. Hanlon KS, Cheng M, Ferrer RM, Ryu JR, Lee B, De La Cruz D, et al. In vivo selection in non-human primates identifies AAV capsids for on-target CSF delivery to spinal cord. Mol Ther. 2024;32:2584–603.
18. Morrison BM, Tsingalia A, Vidensky S, Lee Y, Jin L, Farah MH, et al. Deficiency in monocarboxylate transporter 1 (MCT1) in mice delays regeneration of peripheral nerves following sciatic nerve crush. Exp Neurol. 2015;263:325–38.
19. Wu J, Williams JP, Rizvi TA, Kordich JJ, Witte D, Meijer D, et al. Plexiform and dermal neurofibromas and pigmentation are caused by Nf1 loss in desert hedgehog-expressing cells. Cancer Cell. 2008;13:105–16.
20. Ribeiro S, Napoli I, White IJ, Parrinello S, Flanagan AM, Suter U, et al. Injury signals cooperate with Nf1 loss to relieve the tumor-suppressive environment of adult peripheral nerve. Cell Rep. 2013;5:126–36.
21. Rizvi TA, Akunuru S, de Courten-Myers G, Switzer RC 3rd, Nordlund ML, et al. Region-specific astrogliosis in brains of mice heterozygous for mutations in the neurofibromatosis type 1 (Nf1) tumor suppressor. Brain Res. 1999;816:111–23.
22. Hinderer C, Katz N, Buza EL, Dyer C, Goode T, Bell P, et al. Severe toxicity in nonhuman primates and piglets following high-dose intravenous administration of an adeno-associated virus vector expressing human SMN. Hum Gene Ther. 2018;29:285–98.
23. Huang Q, Chen AT, Chan KY, Sorensen H, Barry AJ, Azari B, et al. Targeting AAV vectors to the central nervous system by engineering capsid-receptor interactions that enable crossing of the blood-brain barrier. PLoS Biol. 2023;21:e3002112.
24. Kawabata H, Konno A, Matsuzaki Y, Sato Y, Kawachi M, Aoki R, et al. Improving cell-specific recombination using AAV vectors in the murine CNS by capsid and expression cassette optimization. Mol Ther Methods Clin Dev. 2024;32:101185.
25. Beharry A, Gong Y, Kim JC, Hanlon KS, Nammour J, Hieber K, et al. The AAV9 variant capsid AAV-F mediates widespread transgene expression in nonhuman primate spinal cord after intrathecal administration. Hum Gene Ther. 2022;33:61–75.
26. Huang Q, Chen AT, Chan KY, Sorensen H, Barry AJ, Azari B, et al. Targeting AAV vectors to the CNS via de novo engineered capsid-receptor interactions. bioRxiv. 2022:2022.10.31.514553.
27. Akalu A, Roth JM, Caunt M, Policarpio D, Liebes L, Brooks PC. Inhibition of angiogenesis and tumor metastasis by targeting a matrix immobilized cryptic extracellular matrix epitope in laminin. Cancer Res. 2007;67:4353–63.
28. Jiang M, Chen M, Liu N. Interactions between Schwann cell and extracellular matrix in peripheral nerve regeneration. Front Neurol. 2024;15:1372168.
29. Dodd RD, Mito JK, Eward WC, Chitalia R, Sachdeva M, Ma Y, et al. NF1 deletion generates multiple subtypes of soft-tissue sarcoma that respond to MEK inhibition. Mol Cancer Ther. 2013;12:1906–17.
30. Stemmer-Rachamimov AO, Louis DN, Nielsen GP, Antonescu CR, Borowsky AD, Bronson RT, et al. Comparative pathology of nerve sheath tumors in mouse models and humans. Cancer Res. 2004;64:3718–24.
31. Kershner LJ, Choi K, Wu J, Zhang X, Perrino M, Salomonis N, et al. Multiple Nf1 Schwann cell populations reprogram the plexiform neurofibroma tumor microenvironment. JCI Insight. 2022;7:e154513.
32. Bohlen MO, McCown TJ, Powell SK, El-Nahal HG, Daw T, Basso MA, et al. Adeno-associated virus capsid-promoter interactions in the brain translate from rat to the nonhuman primate. Hum Gene Ther. 2020;31:1155–68.
33. Powell SK, Samulski RJ, McCown TJ. AAV capsid-promoter interactions determine CNS cell-selective gene expression in vivo. Mol Ther. 2020;28:1373–80.

34. Gonzalez-Sandoval A, Pekrun K, Tsuji S, Zhang F, Hung KL, Chang HY, et al. The AAV capsid can influence the epigenetic marking of rAAV delivered episomal genomes in a species dependent manner. Nat Commun. 2023;14:2448.
35. Okada Y, Hosoi N, Matsuzaki Y, Fukai Y, Hiraga A, Nakai J, et al. Development of microglia-targeting adeno-associated viral vectors as tools to study microglial behavior in vivo. Commun Biol. 2022;5:1224.
36. McKee KK, Yang DH, Patel R, Chen ZL, Strickland S, Takagi J, et al. Schwann cell myelination requires integration of laminin activities. J Cell Sci. 2012;125:4609–19.
37. Skoumal M, Seidlits S, Shin S, Shea L. Localized lentivirus delivery via peptide interactions. Biotechnol Bioeng. 2016;113:2033–40.
38. Chan KY, Jang MJ, Yoo BB, Greenbaum A, Ravi N, Wu WL, et al. Engineered AAVs for efficient noninvasive gene delivery to the central and peripheral nervous systems. Nat Neurosci. 2017;20:1172–9.
39. Drouyer M, Chu TH, Labit E, Haase F, Navarro RG, Nazareth D, et al. Novel AAV variants with improved tropism for human Schwann cells. Mol Ther Methods Clin Dev. 2024;32:101234.
40. Zincarelli C, Soltys S, Rengo G, Rabinowitz JE. Analysis of AAV serotypes 1-9 mediated gene expression and tropism in mice after systemic injection. Mol Ther. 2008;16:1073–80.
41. Romo CG, Piotrowski AF, Campian JL, Diarte J, Rodriguez FJ, Bale TA, et al. Clinical, histological and molecular features of gliomas in adults with neurofibromatosis type 1. Neuro Oncol. 2023;25:1474–86.
42. Wilson JM, Flotte TR. Moving Forward After Two Deaths in a Gene Therapy Trial of Myotubular Myopathy. Hum Gene Ther. 2020;31:695–6.
43. Hordeaux J, Lamontagne RJ, Song C, Buchlis G, Dyer C, Buza EL, et al. High-dose systemic adeno-associated virus vector administration causes liver and sinusoidal endothelial cell injury. Mol Ther. 2024;32:952–68.
44. Xie J, Xie Q, Zhang H, Ameres SL, Hung JH, Su Q, et al. MicroRNA-regulated, systemically delivered rAAV9: a step closer to CNS-restricted transgene expression. Mol Ther. 2011;19:526–35.
45. Krolak T, Chan KY, Kaplan L, Huang Q, Wu J, Zheng Q, et al. A high-efficiency AAV for endothelial cell transduction throughout the central nervous system. Nat Cardiovasc Res. 2022;1:389–400.

ACKNOWLEDGEMENTS

We thank Dr. Akiko Yoshinaga for help with genotyping of the neurofibroma model and professional insights into NF1, Ms Suzanne McDavitt for skilled editorial assistance and Ms Diane M. Nguyen for assistance with figure artwork. We thank Dr. Judith S. Kempfle for the recommendation of the anti-Sox10 antibody for the immunofluorescence experiment. We thank Dr. Nancy Ratner for providing $Nf1^{flox/flox}$ mice and helpful review of the manuscript. We thank Dr. K.A. Kleopa for helpful discussion around the timing of the in-life mouse AAV gene transfer experiments.

AUTHOR CONTRIBUTIONS

C.A.M., K.S.H. and X.O.B. conceived of the study, analyzed data, and wrote the manuscript. C.A.M. performed all of the tail vein injections of mice and assisted in tissue harvesting. S.P., P.S.C., C.C.D.H. and E.A.H. maintained the mice colony, breeding, genotyping, sciatic nerve injections, perfusion, and sacrifice of the mice for further analysis. A.S.R. carried out the pathological analyses in collaboration with S.P. and E.A.H. E.A.H. performed the RT-ddPCR analysis on neurofibroma and confocal microscopy. P.E. performed confocal microscopy and image analysis on the neurofibroma from mice injected with the different AAV vectors. N.P. cloned the AAV-P0-tdTomato construct. D.D.L.C. and A.V.C. produced, purified, and titered all AAV vectors used in the study, C.N. and G.W.R. performed cryosectioning of nerves and the immunofluorescence staining of neurofibroma sections. A.C. provided the luciferase floxed mouse model and advised on the study. M.C. assisted with image analysis. I.C.H, S.M. and N.J. performed microscopy analyses. All authors helped edit, revise, and approve of the manuscript.

FUNDING

This work was supported by NIH R01 grant DC017117 (C.A.M.), the Gilbert Family Foundation Award #521015 (C.A.M.) and the Gilbert Family Foundation Award #521013 (X.O.B.). I.C.H is supported in part by the National Institute of Biomedical Imaging and Bioengineering under award number 1K25EB032864-01A1.

COMPETING INTERESTS

CAM has a financial interest in Sphere Gene Therapeutics, Inc., Chameleon Biosciences, Inc., and Skylark Bio, Inc., companies developing gene therapy platforms. CAM's interests were reviewed and are managed by MGH and Mass General Brigham in accordance with their conflict-of-interest policies.

ETHICAL APPROVAL

All animal procedures were performed in accordance with Massachusetts General Hospital's (MGH's) recommendations for the care and use of animals and were maintained and handled under protocols approved by the Institutional Animal Care and Use Committee (IACUC).

ADDITIONAL INFORMATION

Supplementary information The online version contains supplementary material available at https://doi.org/10.1038/s41434-025-00542-9.

Correspondence and requests for materials should be addressed to Xandra O. Breakefield or Casey A. Maguire.